A Positioning System and Position Control System of a Quad Rotor Applying Kalman Filter to an UWB Module and an IMU

Shota Nakamura[1], Yoshiyuki Higashi[2], Arata Masuda[3] and Nanako Miura[4]

Abstract— **In this paper, the method of controlling the position of the quad rotor was shown aiming structure inspection. The data obtained from an ultra-wide band (UWB) module capable of measuring a distance, an inertial measurement unit (IMU), and a distance sensor were fused and passed through a Kalman filter to estimate three-dimensional coordinates. All calculation of the position coordinates was performed in the on-board computer of the quad rotor, and the computer from the outside gave only the start command of position control. In order to verify the position estimation accuracy and the position control performance, we carried out the position hold hovering experiment at one point and experiment to move multiple points. The possibility of the position estimation and the position control using the UWB module and the IMU was shown.**

I. INTRODUCTION

In Japan's current social infrastructure, the progress of aging is a serious problem. Among them, especially in the case of bridges, those with a length of more than 15 m were present at 400,000 bridges in 2013. Among them, the percentage of those 50 years after construction accounts for 18%[1]. As these aging bridges are expected to increase further in Japan in the future, it is an urgent task in Japan to inspect them properly. However, local governments that manage these bridges lack the labor cost required for inspection, the cost of equipment, and engineers who inspect them. Furthermore, it is needless to say that Japan will have a declining birthrate and an aging society in the future, and more financial resources and human resources will be lacking.

Therefore, there is a need for development of a bridge inspection robot that reduces labor cost and simplifies inspection methods. There are two ways to approach the inspection points. First, it is a way to approach from the ground. As shown in [2], there is an inspection robot equipped with magnets at the end of the wheels, and it can travel to the inspection points through the metal beams and floors. However, there are problems. When this robot goes to the inspection points, all roads need to be connected without gaps, and there must be no obstacles. Second is to approach from the sky. If the robot can fly to the inspection points, it can avoid obstacles unlike the ground-based robot, and the route to the inspection points need not to be continuous. Therefore, in this research, we aimed to develop a method that can inspect bridges using a quad rotor. In previous studies, the quad rotor equipped with the magnet, which is called EPM (Electro-Permanent Magnet) and can control magnetization and separation, and with the movable arm was developed. It can stick to the steel frames and inspect the back side of the steel frames with the arm[3]. However, there are also some challenges in using UAV for inspection.

The UAV can avoid obstacles, however it requires the skill of the pilot. Also, if the UAV gets into the other side of the structure, it becomes extremely difficult to maneuver as it will not be visible to the pilot. Therefore, there is methods of semi automatic or fully automatic position control of a UAV using a position estimation system such as GPS[4][5][6]. However, positioning methods using GPS radio waves can not receive radio waves if the UAV goes under the structures, and making positioning impossible. There are also camera-based positioning methods such as SLAM[7], however expensive and heavy cameras need to be loaded on the UAV, or it is necessary to use an external computer to perform heavy burden calculations. Previous research has described the method of positioning the quad rotor referenced in this paper[8]. However, in that research, it was not achieved to control the position of the quad rotor based on the position coordinates estimated from the method.

So, in this research, the data obtained from the UWB module which can measure the range and the IMU mounted on the quad rotor are fused. And the position estimation method of the quad rotor is shown by applying them to a Kalman filter. A method is also proposed to control the position of the quad rotor even in non-GPS environments.

From the next chapter, we first describe the method of estimating the position in a non-GPS environment and then describe the method of position control using that estimated values. Then, the accuracy of the position estimation and the performance of the position control are verified by the some experiments. Finally, the conclusion is stated.

II. THE NUMERICAL MODEL OF THE QUAD-ROTOR

A. Coordinate System and Rotation Matrix

The position estimation method of the quad rotor shown in this chapter is based on [8]. Fig. 1 shows the coordinate system of the quad rotor. The first coordinate system is the reference frame (r-frame). The r-frame is an earth-fixed inertial frame. The second coordinate system is the body frame (b-frame). The b-frame is a body-fixed frame whose

[1]Shota Nakamura, Division of Mechanodesign, Kyoto Institute of Technology, Kyoto 606-8585 m8623117@edu.kit.ac.jp

[2]Yoshiyuki Higashi, Faculty of Mechanical Engineering, Kyoto Institute of Technology, Kyoto 606-8585 higashi@kit.ac.jp

[3]Arata Masuda, Faculty of Mechanical Engineering, Kyoto Institute of Technology, Kyoto 606-8585 masuda@kit.ac.jp

[4]Nanako Miura, Faculty of Mechanical Engineering, Kyoto Institute of Technology, Kyoto 606-8585 miura-n@kit.ac.jp

origin o^b is at the center of gravity of the quad rotor. The absolute position of the quad rotor is defined by $\mathbf{p_r} = [x, y, z]^T$ and the attitude of the quad rotor is defined by three Euler angles, $\Theta = [\phi, \theta, \psi]^T$. In order to translate vector from b-frame to r-frame, the orthogonal rotation matrix is used (1).

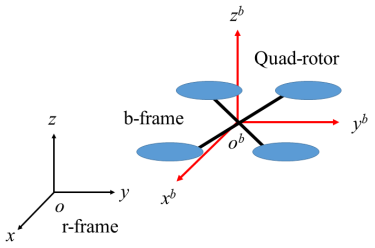

Fig. 1. Coordinate system of the quad rotor

$$\mathbf{R} = \begin{bmatrix} c\theta c\psi & c\theta s\psi & -s\theta \\ s\phi s\theta c\psi & s\phi s\theta s\psi + c\phi c\psi & s\phi c\theta \\ c\phi s\theta c\psi & c\phi s\theta s\psi - s\phi c\psi & c\phi c\theta \end{bmatrix}, \tag{1}$$

where s represents sin, c represents cos. Applying the rotation matrix $\mathbf{R}$, the accelerations on the r-frame $\mathbf{a_r}$ are:

$$\mathbf{a_r} = \frac{d}{dt}\mathbf{v_r} = \mathbf{R}\mathbf{a_b} - \mathbf{g_r}, \tag{2}$$

where $\mathbf{g_r} = [0, 0, -g]^T$ and g is the gravity acceleration and $\mathbf{a_b} = [a_{bx}, a_{by}, a_{bz}]^T$ is the accelerations on the b-frame. The relation between Euler angles and the angular velocity $\omega = [p, q, r]^T$ is:

$$\frac{d}{dt}\Theta = \mathbf{W}\omega, \tag{3}$$

where

$$\mathbf{W} = \begin{bmatrix} 1 & \sin\phi\tan\theta & \cos\phi\tan\theta \\ 0 & \cos\phi & -\sin\phi \\ 0 & \sin\phi\sec\theta & \cos\phi\sec\theta \end{bmatrix}. \tag{4}$$

B. Inertial Measurement Unit (IMU)

Assuming that the quad rotor fly at low speed, $\mathbf{a_r}$ can be ignored. By transforming (2), $\mathbf{a_b}$ is:

$$\mathbf{a_b} = \mathbf{R}\mathbf{g_r} = \begin{bmatrix} g\sin\theta \\ -g\cos\theta\sin\phi \\ -g\cos\theta\cos\phi \end{bmatrix}. \tag{5}$$

Equation (5) expresses the relationship between $\mathbf{a_b}$ and Euler angle.

C. Ultra Wide Band (UWB)

UWB is a wireless system capable of high-speed communication by spreading power over a wide bandwidth. The frequency band to be used is 3.1 GHz to 10.6 GHz, and the bandwidth is 7.5 GHz, which is wider than several hundreds kHz of the conventional radio and 20 MHz of Wi-Fi. Due to the wide bandwidth, it has high ranging accuracy on the order of several 10 cm[9]. Fig. 2 shows ranging protocol of the UWB module. There are three messages, Poll, Response, and Final, exchanged between the quad-rotors and the anchors to get the correct distance. It is calculated based on the quad rotor (T_{RP},T_{SR}, T_{RF}) and the anchor (T_{SP},T_{RR},T_{SF}) timestamps as shown in Fig. 3. With these timestamps, the time taken by radio wave communication, ToF is:

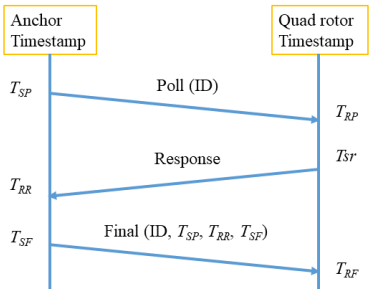

Fig. 2. Ranging protocol of the UWB module

$$ToF = \frac{1}{4}((T_{SP} - T_{RR}) - (T_{SR} - T_{RP}) \tag{6}$$

$$+(T_{RF} - T_{SR}) - (T_{SF} - T_{RR})). \tag{7}$$

The distance between the quad rotor and the anchor, d is obtained by multiplying ToF by the speed of light c.

$$d = ToF \times c. \tag{8}$$

As mentioned in [10], although UWB distance measurement is accurate even near reflectors such as walls, in outdoor environments where structures are dense or in narrow indoor environments, radio waves are reflected by obstacles, and multiple paths occur. The following experiment is an experimental result when an outlier occurs due to multi path. The UWB of one tag was placed on the floor, the four anchors were moved from 1 m to 5 m by 1 m, and the distances between UWBs were measured. Here, there is an error of several tens of centimeters between the distance measured by UWB and the actual distance, so this error was corrected in advance by calibration. The results shown in the Fig. 3 and Fig. 4 were obtained.

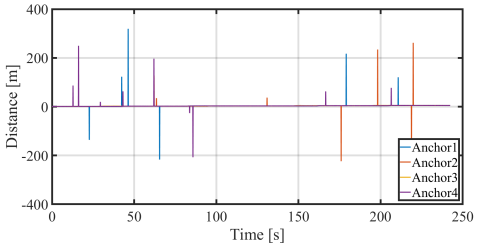

Fig. 3. Ranging result when outliers occur

It can be seen that although distances were measured only at a maximum distance of 5 m, distances exceeding 100 m and distances with negative values occur. The outliers due to this multi path were excluded by filtering by the program.

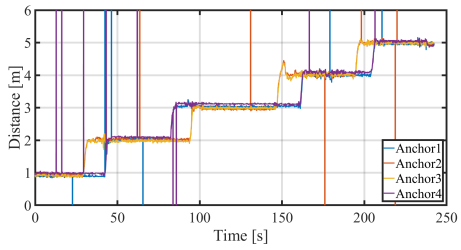

Fig. 4. Ranging result when outliers occur (enlarged image above)

In this filtering method, data measured by UWB is stored temporarily in a buffer, and if there is a change above the threshold when the next data arrives, that value is ignored. Fig. 5 shows the results of those that passed this filtering process in the same experiment.

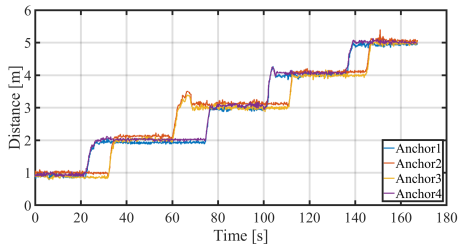

Fig. 5. Ranging results that passed through the filter

It is shown by this experiment that if no outliers occur due to multi path, the distance measurement performance of UWB is high although the measured values are somewhat different depending on the difference of anchors.

Next, a method of estimating the position of the quad rotor using values measured by UWB module will be shown. Here, when the coordinates of the anchors of the four UWB modules are known, the distances d between the respective anchors and the tag are respectively obtained by the following equations.

$$\begin{bmatrix} d_1 \\ d_2 \\ d_3 \\ d_4 \end{bmatrix} = \begin{bmatrix} \sqrt{(x-x_1)^2+(y-y_1)^2+(z-z_1)^2} \\ \sqrt{(x-x_2)^2+(y-y_2)^2+(z-z_2)^2} \\ \sqrt{(x-x_3)^2+(y-y_3)^2+(z-z_3)^2} \\ \sqrt{(x-x_4)^2+(y-y_4)^2+(z-z_4)^2} \end{bmatrix} \tag{9}$$

Solving this equation for the absolute coordinates $\mathbf{p_r} = (x,y,z)^T$ makes it possible to determine the position from the distances between the UWD anchors and tag on the quad rotor, d_1, d_2, d_3 and d_4.

D. Construction of Process Model

The velocity of the quad rotor is defined as $\mathbf{v_r} = [v_x, v_y, v_z]^T$. The relationship between the absolute coordinates $\mathbf{p_r} = [x,y,z]^T$ and the velocity $\mathbf{v_r} = [v_x, v_y, v_z]^T$ is expressed as follows:

$$\frac{d}{dt}\mathbf{p_r} = \mathbf{v_r} \tag{10}$$

We define the state vector as $\mathbf{x} = [\Theta, \mathbf{p_r}, \mathbf{v_r}]^T$; the state space is derived as

$$\frac{d}{dt}\mathbf{x}(t) = \mathbf{f}(\mathbf{x}(t)), \tag{11}$$

The matrix $\mathbf{f}(\mathbf{x}(t))$ in this equation are defined as

$$\mathbf{f}(\mathbf{x}) = \begin{bmatrix} \mathbf{W}\omega \\ \mathbf{v_r} \\ \mathbf{R}\mathbf{a_b} - \mathbf{g_r} \end{bmatrix}. \tag{12}$$

where $\mathbf{x}(t)$ is the state value after t steps and Δt is the sampling time. The following equation is obtained by discretizing this equation using the Euler method. Considering $\mathbf{f}_t(\mathbf{x}(t)) = \mathbf{x}(t) + \mathbf{f}(\mathbf{x}(t))\Delta t$ and $\mathbf{w}_t = \mathbf{w}\Delta t$ the discrete time space equation is derived as:

$$\mathbf{x}(t+1) = \mathbf{f}_t(\mathbf{x}(t)) + \mathbf{w}_t. \tag{13}$$

The measurement equation is obtained from (5)(6)(9).

$$\mathbf{y}(t) = \mathbf{h}_t(\mathbf{x}(t)) + \mathbf{v}_t, \tag{14}$$

where $\mathbf{y}(t) = [a_{bx}, a_{by}, a_{bz}, d_h, d_1, d_2, d_3, d_4]^T$ is output values obtained from each sensor and $\mathbf{v}_t$ is the observation noise. Here $d_h$represents output of distance sensor. The matrix $\mathbf{h}_t(\mathbf{x}(t))$ in this equation are defined as

$$\mathbf{h}_t(\mathbf{x}(t)) = \begin{bmatrix} g\sin\theta \\ -g\cos\theta\sin\phi \\ -g\cos\theta\cos\phi \\ z \\ \sqrt{(x-x_1)^2+(y-y_1)^2+(z-z_1)^2} \\ \sqrt{(x-x_2)^2+(y-y_2)^2+(z-z_2)^2} \\ \sqrt{(x-x_3)^2+(y-y_3)^2+(z-z_3)^2} \\ \sqrt{(x-x_4)^2+(y-y_4)^2+(z-z_4)^2} \end{bmatrix}. \tag{15}$$

From the above, the discrete process model of the system composed of the state equation of (11) and the observation equation of (15) is derived. At the next section, we will show how to estimate the position by applying the extended Kalman filter to this process model.

E. System Implementation

The quad rotor used in this study is shown in Fig. 6. The hardware design of the quad rotor is shown in Fig. 7. The quad rotor is equipped with Tag, which is the mobile station side of the UWB module, and processes data with the Arduino Pro Mini. The NAVIO2 is equipped with various 9-axis sensors and pressure sensors, and is used as a sensor board. In addition, the value of the distance sensor is also used to improve the accuracy of the estimated height. The flight controller (Pixracer) is responsible for attitude control

of the quad rotor. All calculations such as the position estimate and the target angle are performed on the Linux board (Raspberry Pi), and the PWM command value is finally sent to the flight controller. The detailed system relationship diagram is shown in Fig. 8.

Fig. 6. Quad rotor equipped with various sensors, flight controller, and UWB module

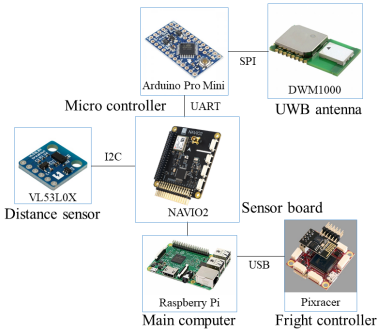

Fig. 7. Hardware design

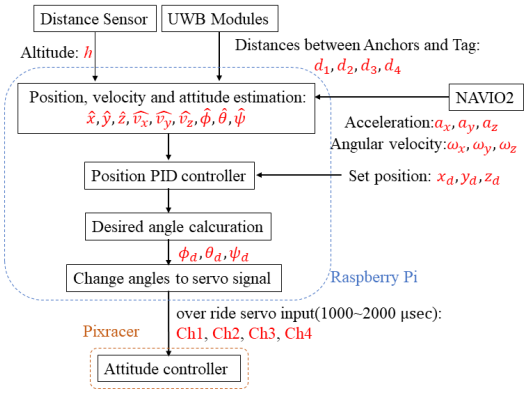

Fig. 8. System core design

III. Sensor fusion algorithm using Extend Kalman Filter (EKF)

The Kalman filter is a kind of infinite impulse response filter for estimating or controlling the state of a dynamic system using observation values including errors. The Kalman filter is used to estimate the time-varying quantity, e.g. the position and velocity of an object, from observations including discrete errors. It is widely used in the field of engineering such as radar and computer vision. For example, in car navigation system, it is applied to integrate erroneous information from a built-in accelerometer or a satellite to estimate the location of a car that changes from moment to moment. The Kalman filter can estimate the position of the target now, in the future, and in the past, utilizing the rules governing the temporal change of the target. Next, the extended Kalman filter is explained. Extended Kalman filter is a method of linearizing nonlinear system at each time using Taylor series expansion, and adapting time-varying Kalman filter at each time.

$\mathbf{f}(\cdot)$, $\mathbf{h}(\cdot)$ are the nonlinear function from the nonlinear system. Jacobian can be used for the linearization like below:

$$\mathbf{A}(t) = \left.\frac{\partial \mathbf{f}(\mathbf{x})}{\partial \mathbf{x}}\right|_{\mathbf{x}=\hat{\mathbf{x}}(t)} \tag{16}$$

$$\mathbf{C}^{\mathrm{T}}(t) = \left.\frac{\partial \mathbf{h}(\mathbf{x})}{\partial \mathbf{x}}\right|_{\mathbf{x}=\hat{\mathbf{x}}^{-}(t)} \tag{17}$$

Then, the estimated value is updated using the following equations. In addition, updating of estimated values is performed through two processes of prediction step and filtering step.

$$\hat{\mathbf{x}}^{-}(t) = \mathbf{f}(\hat{\mathbf{x}}(t-1)) \tag{18}$$

$$\mathbf{P}^{-}(t) = \mathbf{A}(t-1)\mathbf{P}(t-1)\mathbf{A}^{\mathrm{T}}(t-1) + \mathbf{B}\mathbf{Q}\mathbf{B}^{\mathrm{T}} \tag{19}$$

$$\hat{\mathbf{x}}(t) = \hat{\mathbf{x}}^{-}(t) + \mathbf{g}(t)(\mathbf{y}(t) - \mathbf{h}(\hat{\mathbf{x}}^{-}(t))) \tag{20}$$

$$\mathbf{P}(t) = (\mathbf{I} - \mathbf{G}(t)\mathbf{C}^{\mathrm{T}}(t))\mathbf{P}^{-}(t) \tag{21}$$

$$\mathbf{G}(t) = \mathbf{P}^{-}(t)\mathbf{C}^{\mathrm{T}}(\mathbf{C}\mathbf{P}^{-}(t)\mathbf{C}^{\mathrm{T}} + \mathbf{R})^{-1} \tag{22}$$

In the prediction step, using the estimated value $\hat{\mathbf{x}}$ one step ago and the covariance matrix $\mathbf{P}(t-1)$ of the error, the prior estimated value $\hat{\mathbf{x}}^{-}(t)$ at the current time and the prior error covariance matrix $\mathbf{P}^{-}(t)$ are obtained. Then, in the filtering step, the posterior estimated value $\hat{\mathbf{x}}(t)$ up to the current time and the posterior error covariance matrix $\mathbf{P}(t)$ are obtained using $\hat{\mathbf{x}}^{-}(t)$ and $\mathbf{P}^{-}(t)$.

IV. Position Controller

In this chapter, we explain how to control the position of the quad rotor based on the position coordinates described in the previous chapter. This method of controlling the position of the quad rotor is detailed in [11], [12]and[13]. First, using the estimated position coordinates and target coordinates, the virtual input is given by the following equation.

$$U_x = k_{px}(x_d - \hat{x}) + k_{dx}(\dot{x}_d - \dot{\hat{x}}_d) + k_{ix}\int_0^t (x_d - \hat{x})d\tau \tag{23}$$

$$U_y = k_{py}(y_d - \hat{y}) + k_{dy}(\dot{y}_d - \dot{\hat{y}}_d) + k_{iy}\int_0^t (y_d - \hat{y})d\tau \tag{24}$$

As you can see from the equation, this equation represents a PID controller. Then, from the following two equations, the input values of the desired pitch angle and roll angle can be obtained using the above virtual inputs.

TABLE I

ABSOLUTE POSITION OF ANCHORS

	x position [m]	y position [m]	z position [m]
Anchor1	-3.50	2.00	1.82
Anchor2	3.50	2.00	1.82
Anchor3	3.50	-2.00	1.82
Anchor4	-3.50	-2.00	1.82

TABLE II

ABSOLUTE POSITION OF TARGET POINTS

	x position [m]	y position [m]
Point0 (origin)	0.00	0.00
Point1	4.00	0.00
Point2	4.00	-3.00
Point3	0.00	-3.00

$$\phi^{des} = \frac{1}{g}(U_x \sin\psi - U_y \cos\psi) \tag{25}$$

$$\theta^{des} = \frac{1}{g}(U_x \cos\psi + U_y \sin\psi). \tag{26}$$

Finally, the pitch and roll angles are converted to PWM signals. And it is possible to control the position of the quad rotor on the xy plane by overriding these values to the channels of each pitch and roll angle of the transmitter. Also, control in the z-axis direction, that is, altitude control, is possible by implementing a PID controller using error in estimated height and desired height, as in position control on the xy plane. However, as will be described later, in this research, altitude control was not operated automatically but was steered manually, in order to prevent crashing to the ground or hitting the ceiling if the control did not work well.

V. EVALUATION

In this chapter the possibilities of the system was evaluated. First, the position of the quad rotor at rest was estimated using the position estimation method described above, and compared with the true value. Next, experiments were conducted to control the position of the quad rotor using the position estimation method and position control method.

A. Verification of position estimation accuracy

The following TABLE I shows the absolute coordinates of each UWB anchors. First, we measured the distance to the floor of the laboratory exactly and marked 4 coordinate points. TABLE. II shows the position of target points. Then, the quad rotor was placed on that coordinate point and kept stationary for 20 seconds, and this was repeated at four points. And the coordinates at that time were estimated. Fig.9 shows result.

Because the quad rotor was moved by hand, it deviated from the rectangular route while moving the points. However, it can be seen that a value close to the coordinates of the measurement point can be estimated while the quad rotor is stationary at the measurement point. From this, it can be said that the accuracy of the position estimation method proposed in this research is sufficiently high.

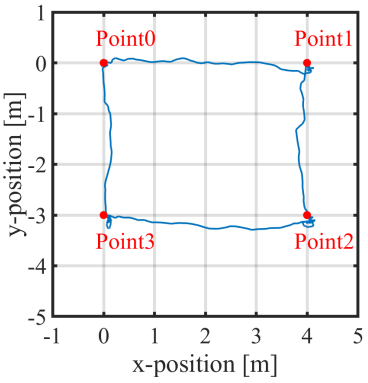

Fig. 9. Coordinates of the quad rotor at rest estimated using the estimation method

B. Static position hold

In this experiment, experiment of position hold at one point was performed. The quad rotor took off by manual operation and switched to automatic operation when it was stable. At first, the quad rotor was placed on the floor and calibrated at the point as the origin in the xy plane, and control was performed to keep it at the origin. The results are shown in Fig. 10. The standard deviation from the center is 0.083 m, and a maximum deviation 0.406 m.

There are two possible causes for the control of the quad rotor to deviate from the set position. First is distance measurement error of the UWB module. The UWB module contains a distance measurement error of several tens of cm. Therefore, it is considered that the ranging error from each of these UWB modules causes an error in position control. Second as shown in the previous chapter, the UWB module estimates the position at about 10 Hz and while the data is not coming from the UWB module, the estimated value is complemented by integrating the IMU data. Therefore, when the quad rotor is at rest, the integral does not significantly affect the position estimation. However, since the acceleration of vibration from the rotor is applied to the IMU during flight, integrating the acceleration including the error adversely affects the position estimation. These two factors affect the position estimation, and it is considered that such an error has occurred.

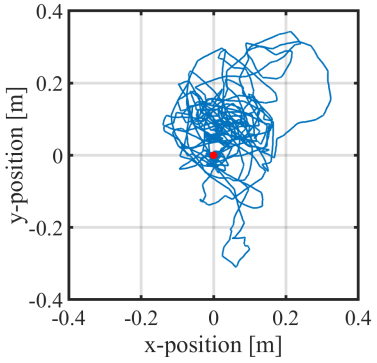

Fig. 10. Result of static position hold experiment for 2 minutes

TABLE III

COORDINATE OF WAY POINTS

	x position [m]	y position [m]
Point0 (origin)	0.0	0.0
Point1	1.5	-1.0
Point2	-1.5	1.0

C. Point to point movement

In this experiment, in addition to the previous static positioning experiment, control was performed to move three coordinates given in advance from point to point. TABLE III shows the coordinate of way points. As in the previous experiment, the point at which the quad rotor was placed was taken as the origin. The target point was switched by switching the toggle switch of the transmitter. Fig. 11 shows the result. The hovering ability at the target point is very similar to the results shown in the previous experiment. The command value was not given during the movement of the point, and only the final target point was commanded. However, the quad rotor was able to reach the target point without straying from the route significantly. It is considered that the deviation can be further reduced if a command value of coordinates is given finely while moving.

In order to further improve the results obtained from these two experiments in the future, it is necessary to use the optical flow sensor data. In the first experiment, the result was that the quad rotor vibrated from the target point and was displaced. This problem can be avoided by obtaining velocity data from the optical flow sensor. The values obtained from the optical flow sensor are the moved velocity on the xy plane. Therefore, it can be said that the speed control can be combined using this value to solve the problem that the quad rotor vibrates resulting from the distance measurement error of UWB. Also, by integrating the velocity data from optical flow sensor, the movement distance can be determined. Therefore, the position estimate accuracy can be improved by incorporating this distance into the position estimating. So, incorporating an optical flow sensor is considered to be effective for the second experiment of moving a plurality of target points.

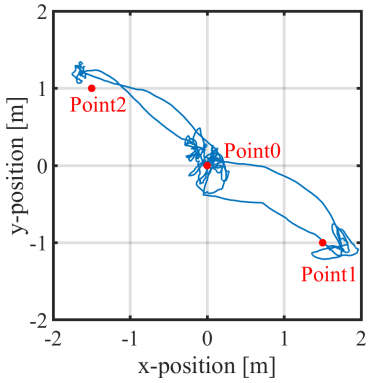

Fig. 11. Result of moving point to point experiment

VI. CONCLUSION

In this paper, research was carried out with the aim of developing a robot that can inspect structures such as bridges even in non-GPS environments. First, we showed how to blend the UWB and IMU data and apply the Kalman filter to estimate the position of the quad rotor. And we showed the method of controlling the position of the quad rotor based on the estimated position coordinate.

Next, two experiments were performed to confirm the accuracy of the position estimation and the position control. The first experiment was the static position hold experiment in which the quad rotor was held at one point. The result showed the standard deviation from the target point is 0.083 m, and the maximum deviation 0.406 m. The second experiment was to control the quad rotor and move the three given points in order. Then, the quad rotor was able to reach the target point without straying from the route significantly while moving between points.

However, in these experiments, it was found that the quad rotor vibrated back and forth from the target point, so that the performance was still insufficient to inspect the structures. In the future, it is necessary to mount a sensor which is able to estimate the velocity in the xy plane such as an optical flow sensor, and to suppress the vibration in the xy plane by controlling the velocity. In addition, it is also effective when moving to a target point by determining the movement distance by integrating speed data and incorporating it in position estimation.

REFERENCES

[1] MLIT, Promotion of infrastructure aging measures, http://www.mlit.go.jp/saiyojoho/manifesto/manifesto7.html (2019/07/20), (in Japanese).

[2] Y. Takada, "Development of a Bridge Inspection Robot Capable of Traveling on Splicing Parts," 2017.

[3] S. Akahori, Y Higashi, A Masuda, "Development of an Aerial Inspection Robot with EPM and Camera Arm for Steel Structures," 2016.

[4] Microdrones, https://www.microdrones.com/en/ (2019/07/20).

[5] ArduCopter, http://ardupilot.org/copter/index.html (2019/07/20).

[6] PHANTOM SERIES, https://www.dji.com/jp/products/phantom (2019/07/20).

[7] M. Blosch, Stephan Weiss, Davide Scaramuzza, and Roland Siegwart, "Vision Based MAV Navigation in Unknown and Unstructured Environments," Robotics and Automation (ICRA), 2010 IEEE International Conference, 21-28, 1010.

[8] S. Aakahori, Y. Higashi, A. Masuda, "Position estimation system using UWB, IMU and Distance Sensor for Quad-rotors," 2017.

[9] DW1000 Radio IC, https://www.decawave.com/product/dw1000-radio-ic/ (2019/07/26).

[10] K. Guo, Z. Qiu, C. Miao, A. Zaini, C. Chen, W Meng, L. Xie, "Ultra-Wideband-Based Localization for Quadcopter Navigation," 2016.

[11] M. L. Ireland, A. Vargas, D. Anderson, "A Comparison of Closed-Loop Performance of Multirotor Configurations Using Non-Linear Dynamic Inversion Control," Aerospace 2015, 2, pp. 325-352.

[12] Z. Zuo, "Quadrotor Trajecotry Tracking Control: A PD Control Algorithm," 2010 3rd International Conference on Computer and Electrical Engineering (ICCEE 2010), 2010.

[13] D. Mellinger, N. Michael and V. Kumar, "Trajectory generation and control for precise aggressive maneuvers with quadrotors," in Experimental Robotics (Springer, 2014) pp. 361 373.